Liu, W., Naydenov, B., Chakrabortty, S., Wuensch, B., Hübner, K., Ritz, S., et al. (2016). Fluorescent Nanodiamond-Gold Hybrid Particles for Multimodal Optical and Electron Microscopy Cellular Imaging. *Nano Letters, 16*(10), 6236-6244. doi:10.1021/acs.nanolett.6b02456.

Fluorescent Nanodiamond-Gold Hybrid Particles for Multimodal Optical and Electron Microscopy Cellular Imaging

Liu, W., Naydenov, B., Chakrabortty, S., Wuensch, B., Hübner, K., Ritz, S., et al.

Fluorescent nanodiamond-gold hybrid particles for multimodal optical and electron microscopy cellular imaging

Weina Liu [1] Boris Naydenov,[2] Sabyasachi Chakrabortty,[1] Bettina Wuensch,[3] Kristina Hübner,[3] Helmut Cölfen,[4] Holger Barth [5], Kaloian Koynov,[6] Haoyuan Qi,[7] Robert Leiter,[7] Rolf Reuter,[8] Jörg Wrachtrup, [9] Felix Boldt,[1] Jonas Scheuer, [2] Ute Kaiser,[7] Miguel Sison,[7] Theo Lasser, [9] Philip Tinnefeld,[3] Fedor Jelezko,[2] Paul Walther, [7] Yuzhou Wu,[1,10] Tanja Weil,[1,6*]*

[1]Department of Organic Chemistry III/Macromolecular Chemistry, Ulm University, Albert-Einstein-Allee 11, 89081 Ulm, Germany. [2]Institute for Quantum Optics, Ulm University, 89081 Ulm, Germany. [3]NanoBioSciences Group, Institute for Physical & Theoretical Chemistry, and Braunschweig Integrated Centre of Systems Biology (BRICS), and Laboratory for Emerging Nanometrology (LENA), Braunschweig University of Technology, 38106 Braunschweig, Germany. [4]University of Konstanz, Physical Chemistry, Universitätsstraße 10, 78457 Konstanz, Germany. [5]Institute of Pharmacology and Toxicology, University of Ulm Medical Center, Albert-Einstein-Allee 11, 89081 Ulm, Germany. [6]Max-Planck-Institute for Polymer Research, Ackermannweg 10, 55128 Mainz, Germany. [7]Central Facility for Electron Microscopy, Ulm University, 89081 Ulm, Germany. [8]Institute of Physics, University of Stuttgart, 70569 Stuttgart, Germany. [9]Laboratoire d'Optique Biomédicale, École Polytechnique Fédérale de Lausanne, BM 5143, Station 17, CH-1015 Lausanne, Switzerland. [10] School of Chemistry and Chemical Engineering, Huazhong University of Science and Technology, 1037 Luoyu Road, 430074, Wuhan, China.

KEYWORDS Nanodiamond, nanogold, hybrid particles, multimodal imaging, lifetime-engineering

ABSTRACT There is a continuous demand for imaging probes offering excellent performance for various imaging techniques to provide comprehensive investigations of cellular processes by more than one technique. Fluorescent nanodiamond-gold hybrid nanoparticles (FND-Au) constitute a new class of "all-in-one" particles providing unique features for multimodal cellular imaging ranging from optical imaging, electron microscopy and potentially even quantum sensing. Confocal and optical coherence microscopy of the FND-Au allow fast investigations inside living cells *via* both emission, scattering and photothermal imaging without quenching of FND emission by Au. In electronic imaging, transmission electron microscopy (TEM) and scanning transmission electron microscopy (STEM) of FND-Au reveal greatly enhanced contrast as well as an extraordinary flickering behavior in three dimensional cellular environments. The unique multimodal imaging characteristics of FND-Au enable detailed studies inside cells ranging from statistical distributions at the entire cellular level down to tracking of individual particles at the low nanometer scale. Herein, the processes of endosomal membrane uptake and release of FNDs were elucidated for the first time by imaging individual FND-Au hybrid nanoparticles with single particle resolution. Their facile preparation, the availability of various surface groups, their flexible detection modalities, single particle contrast in combination with the capability for endosomal escape, and their lacking cytotoxicitymake FND-Au unique candidates for multimodal optical-electronic imaging applications with great potential for emerging techniques such as quantum sensing inside living cells

Fluorescent nanodiamonds (FNDs) constitute an emerging class of three-dimensional, nanosized carbon materials with localized optically active point defects in their crystal lattice. Due to the presence of such defects and the resulting excellent optical properties, FNDs receive an ever-increasing interest in up-front bioimaging applications such as quantum sensing, super-resolution live-cell imaging, and single-particle tracking.[1] Particularly, the nitrogen vacancy (NV) center, a substitutional nitrogen defect in direct vicinity to a vacancy, is the most extensively studied characteristic of FNDs. It offers many advantages for fluorescence imaging such as stable emission, which is resistant to photobleaching,[2] and broad emission wavelength including NIR emission. More importantly, the NV center has a zero-field magnetic resonance between the ms = 0 and the ms = ±1 magnetic states of an electronic spin triplet. This electron spin exhibits remarkably long coherence (T2) and relaxation times (T1), which can reach milliseconds in ultrapure diamond.[3] Thus, even for single NV centers, this electronic spin can be easily detected, which is particularly attractive for quantum sensing in a biological environment to study temperature changes, detect nanoscopic electron spins, or accomplish single-molecular NMR and hyperpolarized magnetic resonance imaging.[4–7] Moreover, FNDs allow high-resolution imaging at the single-nanoparticle level.

One of the most promising applications of FNDs is their use as markers in super-resolution stimulated emission depletion microscopy (STED), which provides single-particle and even single-NV-center resolution fluorescence imaging on glass plates[8] or inside cells.[9] Furthermore, FNDs are based on carbon crystals that are considered biocompatible[10] and stable against enzymatic degradation.[11] Therefore, due to their unique optical and electronic characteristics, FND-Au provides great opportunities to study biological structures and processes with high-precision in vitro and, potentially, also in vivo.

Although FNDs provide several important advantages for various optical microscopy techniques, they have relatively low contrast in electron microscopy, which can represent a

limitation. For example, fluorescence imaging studies indicated that FNDs capable of escaping from endosomes were homogeneously distributed inside the cytosol.[12] The endosomal membrane penetration was attributed to the sharp edge structures of the FNDs,[12] but due to limited resolution in optical imaging, no direct proof was given. Transmission electron microscopy (TEM) provides access to cellular structures with nanometer-scale resolution, which allows analyzing cellular processes such as the membrane translocation of FNDs in greater detail. However, due to the low contrast of FNDs in TEM, it is very challenging to differentiate FNDs from the complicated background in cellular environments.[13] Therefore, the design of hybrid nanoparticles suitable for multimodal imaging by combining different imaging techniques would be highly desirable to ultimately achieve single particle resolution with highest sensitivity in different cellular environments.

Herein, FNDs were decorated with Au nanoparticles (AuNPs) yielding FND-Au hybrid particles (FND-Au) combining the inherent features of each individual nanoparticle. The hybrids were prepared by a controlled protein coating method and exhibited narrow size distributions and long-term stability during storage as well as excellent biocompatibility. The stabilization of single FNDs and AuNPs in one hybrid particle system opens access to multiple detection techniques and improves certain features of the FND-Au. In contrast to the emission quenching of AuNPs in AuNPs−chromophore conjugates, the presence of AuNPs in the FND-Au hybrids did not debilitate the emission properties of the FNDs. AuNPs in the FND-Au nanoparticles even enhanced the emission brightness and shortened the lifetime of the excited state, which offers faster fluorescence imaging at lower laser power. The FND hybrids reported herein were well-distinguishable from the dense subcellular background with high contrast due to the labeling with AuNPs thus facilitating detailed investigations by electron microscopy imaging. In this way, their cellular distribution and penetration of endosomal membranes was studied by TEM, and a unique flickering behavior of the FNDs was recorded by 3D scanning transmission electron microscopy (STEM) for the first time. Due to their excellent optical and

electronic features, their capability of endosomal escape, and high biocompatibility, the FND-Au hybrid particles reported herein represent a powerful platform for studying cellular activity and functions with single-particle resolution, which is challenging to achieve with a single imaging technique

Result and Discussion:

Preparation and Purification of hybrid nanoparticles. To prepare FND-Au hybrid particles suitable for cellular imaging, the following major challenges had to be solved: (1) high tendency of the FNDs to form aggregates in buffer and cell culture medium, (2) limited affinity of AuNPs to adsorb at the FND surface, (3) necessity of attaching only one or two AuNPs per FND, and (4) stabilization of the hybrid particles to allow purification and long-term cellular studies. To achieve these goals, the FND-Au hybrid particles were prepared by adsorption of AuNPs and the human plasma protein human serum albumin[14] (HSA) as multifunctional stabilizer onto FNDs in solution (Fig. 1a, step 1). By careful adjustment of the relative ratios of the FND, AuNPs, and HSA (weight ratio 1:5.7:2), defined hybrid nanoparticles were prepared in aqueous solution (see supporting information for more details). Since AuNPs and HSA were adsorbed to the FNDs non-covalently, the resulting hybrid nanoparticles were still unstable at this stage. Therefore, the carboxylate groups at the surfaces of the FNDs and AuNPs were cross-linked with the amine groups of HSA to stabilize the hybrid nanoparticles by additional covalent linkages (Fig. 1a, step 2). The size distribution of the FND-Au was then further improved by applying ultracentrifugation (Fig. S2a). The analytical ultracentrifugation (AUC) method provides detailed analysis of the FND-Au mixture and the generation of the sedimentation coefficient distribution (s-distribution, Fig. S2b). Through the s-distribution, the nanoparticle size distribution (d-distribution, Fig. 1b) was obtained, from which interdependent parameters, such as rotor angular velocity and centrifugation time, were calculated to ultimately separate the FND-Au within the desired size range. As illustrated in Fig. 1c, fraction ii from Fig. 1b

containing single FNDs with one or two AuNPs attached to the surface were isolated from the crude reaction mixture by preparative ultracentrifugation (UC).

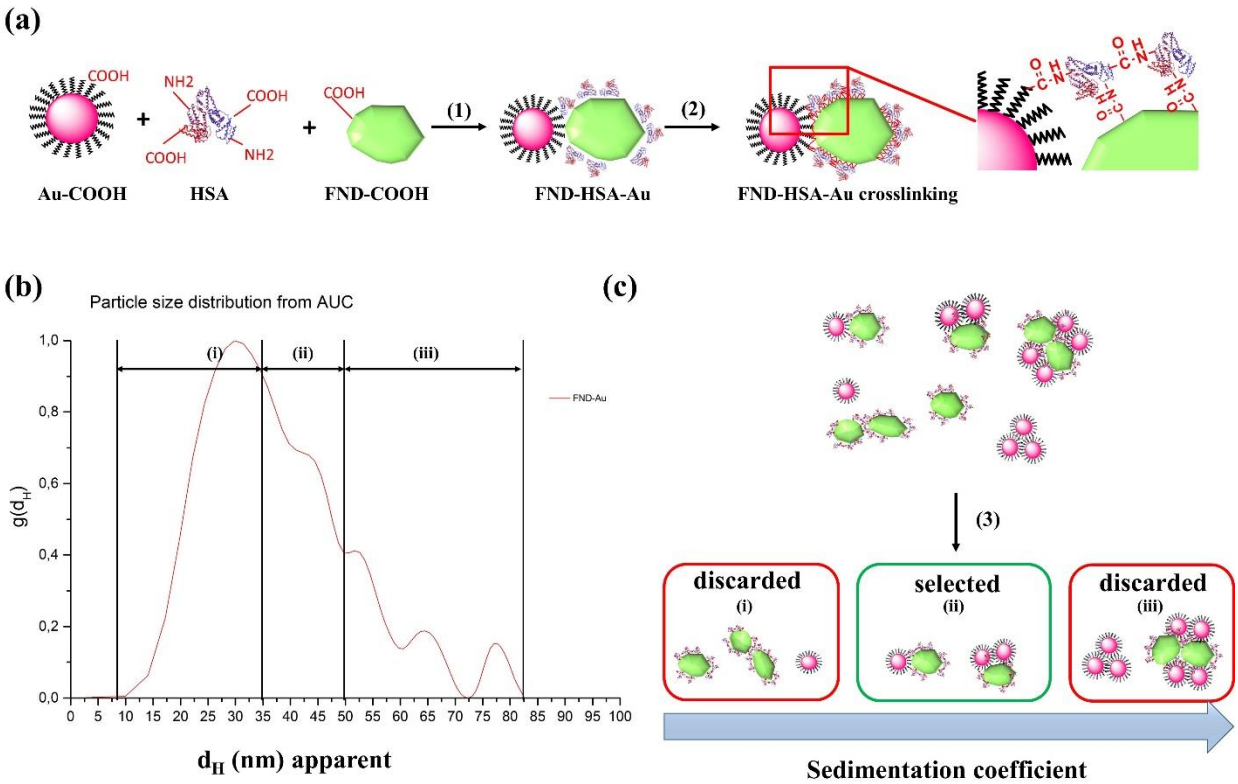

Figure 1. (a) FND-Au preparation through (1) the protein incomplete coating (step 1). (2) EDC/NHS-catalyzed carboxylic and amine crosslinking to stabilize the hybrid nanoparticles (step 2). (b) Nanoparticle size distribution generated by the sedimentation coefficient curve from AUC ($\rho_{solvent}$: 0.99704 g/mol, $\eta_{solvent}$: 0.00891, $\rho_{particle}$: 7.52 g/cm^3, absorbance: 540 nm, speed: 3000 rpm): Only fraction (ii) contained the desired FND-Au within the size range of 35-50 nm. (c) Illustration of the hybrid nanoparticle separation by ultracentrifugation (step 3).

FND-Au Characterization. The isolated fraction (ii) obtained from UC was analyzed by TEM (Fig. 2a), and FND-Au with only one or two AuNPs attached to single FNDs were observed, indicating that unbound AuNPs, FNDs, and larger aggregates were removed successfully (Fig. 2c and d). Quantification of the FND-Au sizes by counting about 300 particles in TEM imaging gave average diameters of about 33 nm with narrow size distributions (Fig. 2a, insert). FNDs with their uneven surface structures only reveal low imaging contrast, and considerably higher contrast was only observed in the presence of the spherical AuNPs. Quantification of the first

successful attachment of AuNPs to the FNDs surface based on TEM imaging indicated about 78% of FND-Au, 19.5% single

The individual FND and AuNPs in the FND-Au hybrids were imaged by high-resolution TEM (HRTEM), revealing their respective characteristic crystal lattice spacing (Fig. 2b). Increased hydrodynamic diameters (Dh) of the FND-Au hybrids of about 50 nm were observed in aqueous suspension by fluorescence correlation spectroscopy (FCS)[15] due to the attachment of the AuNPs to the raw FNDs with diameters of about 33 nm (Fig. 2e). In this way, stable FND-Au nanoparticles with average diameters of about 48 nm according to dynamic light scattering were achieved, with high shelf lives of more than 6 months of storage at 4 °C (Fig. S4a). Moreover, the convenient and reproducible "mixing" protocol even allowed rapid production of larger quantities at the gram scale. In addition, the small distance between the FND and AuNPs of about 1 nm (Fig. 2b) allows the tuning of the optical properties and spin state of the FNDs. Such close FND-nanoparticle distances have not been realized by any otherFND preparation scheme reported yet.

Single-molecule sensitive fluorescence imaging (Fig. 2f) revealed that the AuNPs did not deteriorate the emission brightness of the FNDs, which is a common problem when chromophores are conjugated to AuNPs. The intensity histograms indicated that the FND-Au were, even by a factor of 1.3, brighter than the individual FNDs (Fig. 2g). In parallel, the lifetime of the excited state was reduced by a factor of ~2 (see fluorescence lifetime histograms in Fig. S3) due to coupling of the NV center to the plasmons in the AuNPs nanoparticles, which shortened the lifetime of the excited state and resulted in altered emission.[16–18] Second-order autocorrelation (g(2)) measurements of the FND and FND-Au emission (Fig. 2h) confirmed that the NV in the FND acted indeed as a single photon emitter. The dependence of the emission on the power of the excitation laser was depicted in Fig. 2i. Remarkably, in the linear regime (laser power below 100 μW), the FND-Au hybrids emitted almost four times more photons

compared to the individual FNDs (2.21 versus 0.605 kcounts/μW). These results unambiguously indicated that FND-Au hybrid nanoparticles provide improved features for cellular imaging compared to the results from FNDs because less laser power was required for image acquisition, which should reduce cellular toxicity. By further analyzing the power dependence of the g(2) via a three-level system model,[19] we demonstrated that the lifetime of the excited state of the FND-Au was shortened from 20.8 ns for single FNDs to about 14 ns. These results were comparable with the direct lifetime measurements (see also Fig. S3). The enhanced emission of the FND-Au was attributed to the shortened lifetime of the NV and to the more efficient laser excitation due to the concentration of the exciting light by the AuNPs.

Cellular Uptake and Biocompatibility of FND-Au Hybrid Particles. The application of FND-Au as powerful multi-modal optical imaging platform requires efficient cellular uptake of the hybrid nanoparticles. The first layer HSA coating provides negative net charge at neutral pH (isoelectric point of 5.9)[20] and a high tendency to complex various polymeric polycations. The negative surface charge (zeta potential -22.4 mv, Fig. S4) of the HSA conjugated FND-Au hybrid particles limits cell membrane interactions and cellular uptake.[21] Therefore, following a previously published protocol,[21] the surface charge was converted to positive through complex formation with the biocompatible HSA-derived polyethylene glycol (HSA-PEO) biopolymer (Fig. 3a). In principle, any other polycationic polymer could also be applied. The coated FND-Au hybrid particles revealed positively charged surfaces (zeta potential 28.8 mv, Fig. S4) as well as efficient cellular uptake as shown by confocal microscopy and OCM images in the following.

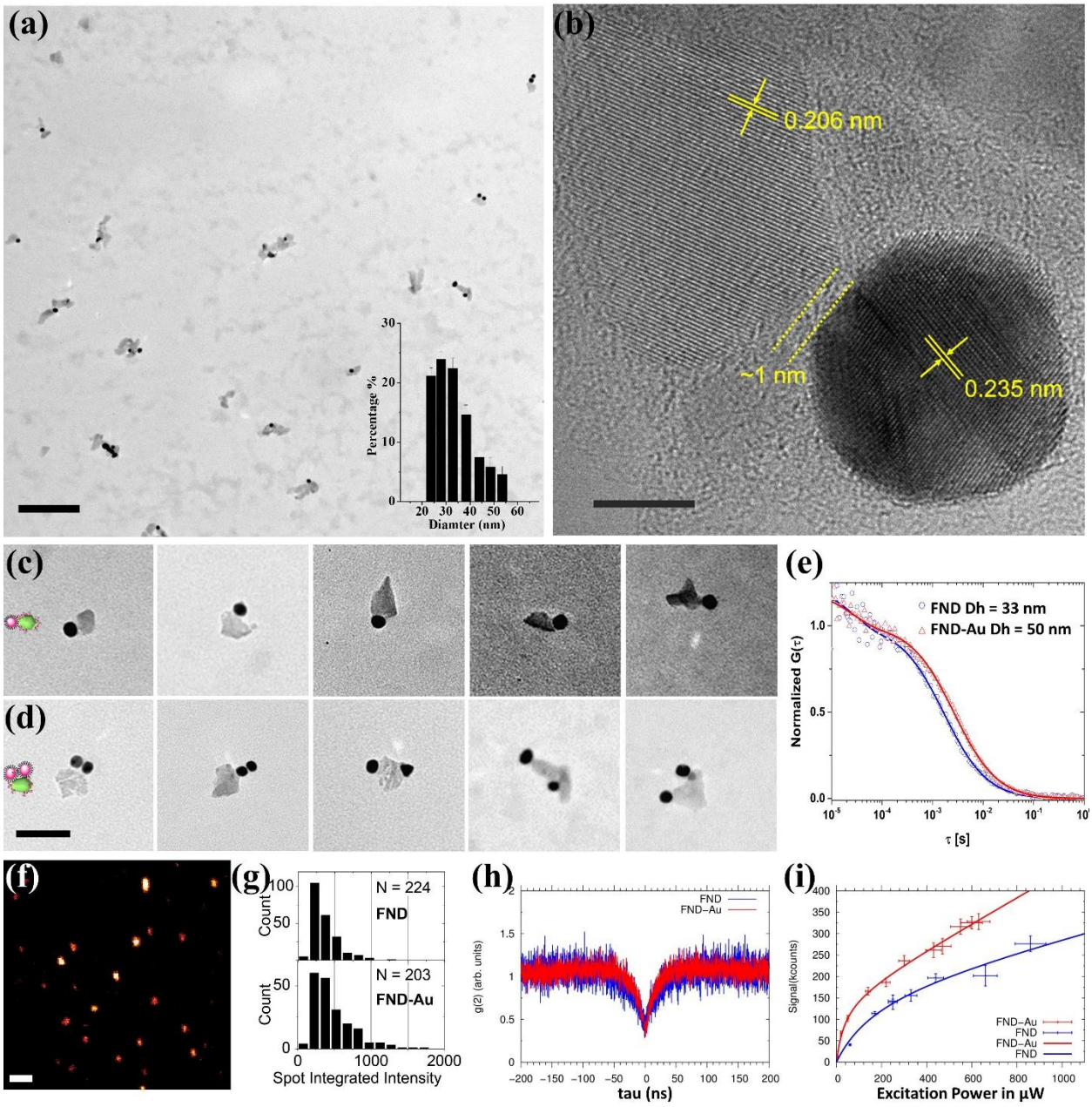

Figure 2. Characterization of FND-Au hybrid particles. (a) TEM image of FND-Au. The insert shows the size distribution of FND-Au. (b) HRTEM image of the FND-Au on graphene supporting film. The lattice fringes of FND(0.206 nm) and Au(0.235 nm) can be clearly resolved. The separation width between the FND and Au was measured to be about 1 nm. (c and d) Representative TEM images of FND-Au_1 and FND-Au_2. (e) Fluorescence correlation spectroscopy autocorrelation curve of FND-Au compared to FND. (f) High resolution confocal image of single FND-Au nanoparticles. (g) Histogram of FND-Au and FND fluorescence spot intensity. (h) Normalized second-order auto-correlation of the fluorescence emitted from FNDs (blue) and FND-Au (red). $g^{(2)}$ at $\tau = 0$ is below 0.5, which is a signature of a single photon emitter. (i) Dependence of the fluorescence on the power of the excitation laser. Scale bar; (a) 200 nm, (b) 5 nm, (c) and (d) 50 nm, (e) and (f) 1µm.

The biocompatibility of FND-Au was evaluated by studying their effect of FND-Au on epithelial cells and macrophages. HeLla cells (human negroid cervix epitheloid carcinoma cell line) and murine macrophages (J774A.1) were incubated with increasing concentrations of FND-Au for 48 h and the cell viability was identifiedrecorded. Staurosporine (stau, 500 nM, an established inducer of apoptotic cell death) was applied as positive control. FND-Au hybrid nanoparticles were found very well tolerated by living cells as demonstrated by their negligible toxcicity in both cell typelines types even inat high concentrations of 1000 µg/mL (Fig. 3b and Fig. S5a). As an incubation of cells with the FND-Au hybrid nanoparticles did not affect the amount of viable cells, the nanoparticles did neither induce cell death nor interfere with cell division. Compared to stau or bacterial lysate containing lipopolysaccharide, As well non-obviousno macrophages activityation was induced by FND-Au, compared with stau or bacterial lysate (Fig. 3c) indicating that FND-Au will most likely not trigger inflammatory reactions upon in vivo applications.

–

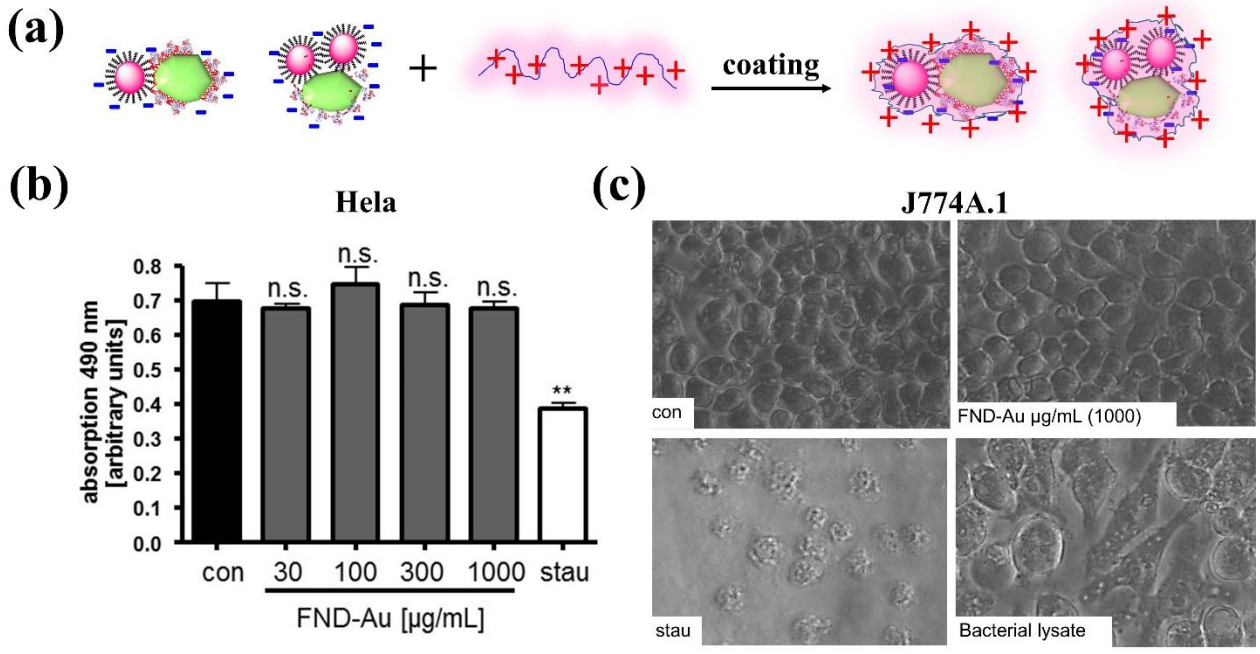

Figure 3. (a) Biopolymer HSA-PEO coated FND-Au. (b) Effect of FND-Au on viability of epithelial cells. c) No effect of FND-Au on macrophage viability and activation.

Cell viability was also evaluated in A549 cells (an adenocarcinomic human alveolar basal epithelial cell line) by investigating the presence of adenosine triphosphate (ATP) over even longer incubation periods. Only at very high concentrations (400 μg/mL) of the FND-Au, which are not relevant for imaging applications,[1,22] cell viability was slightly affected, but still about 75% viable cells remained, even after 72 h incubation at such a high concentration (Fig. S5b). Moreover, incubation with the FND-Au did not result in reactive oxygen species (ROS) formation in human epithelial cells (Fig. S5c). Furthermore, the endocytic machinery was not disturbed in HeLa cells treated with the FND-Au, as demonstrated by the endocytic uptake of a bacterial protein toxin, namely Clostridium botulinum C2 toxin (Fig. S 5d). C2 toxin was taken up into cells by receptor-mediated endocytosis and translocated from early acidified endosomal vesicles into the host cell cytosol, where it modified G-actin and caused cell-rounding.[23] Because there was no obvious difference in the cytotoxic effects induced by C2 toxin in cells treated with FND-Au or not, it was concluded that the uptake of this toxin via endosomes was found to be comparable in untreated and FND-Au treated cells and that FND-Au did not negatively affect endocytotic pathways. In addition, the impact of FND-Au on caspase 3/7 activity was studied in HeLa cells. Again, no effect was observed (Fig. S5e), clearly indicating that the FND-Au were very well tolerated by cells. In comparison to the results from other Au hybrid particles[22,24] reported so far, the cell experiments indicated improved biocompatibility of FND-Au.

FND-Au for intracellular optical microscopy imaging. FND-Au particles were applied for multimodal optical imaging ranging from fluorescence, scattering, and optical coherence microscopy (OCM). A549 cells were incubated with FND-Au (100 μg/mL) for 24 h and then studied by confocal laser scanning microscopy (CLSM, Fig. 4a–c). A549 cells loaded with FND-Au hybrid nanoparticles were imaged in both fluorescence and scattering channels, as depicted in Fig. 4d–f. The scattering channel provided an additional option for FND-Au detection in optical imaging, which is specific for nanoparticles and allows their differentiation

from organic fluorophores. The 84.4% overlap of the emission and scattering images was quantified by the Fiji software (JACoP plugin), indicating the presence of high contents of FND-Au. The minor, nonoverlapping portion was attributed either to FND-Au already dissociated inside cells or to the different sensitivities of these two detection modes. Therefore, to further assess how many FND-Au hybrid particles remained colocalized after cellular uptake and to evaluate the stability of the protein coating, we have lysed the cells and extracted all particles after incubation for different time periods. A549 cells were incubated with FND-Au for 12 and 24 h. Thereafter, the cells were mechanically lysed by high-speed centrifugation and sonication to harvest all nanoparticles that were taken up by the cells.[25] The released nanoparticles were collected and imaged by TEM. Even after 12 h of incubation with cells, high numbers of individual FND-Au hybrid particles were still observed.

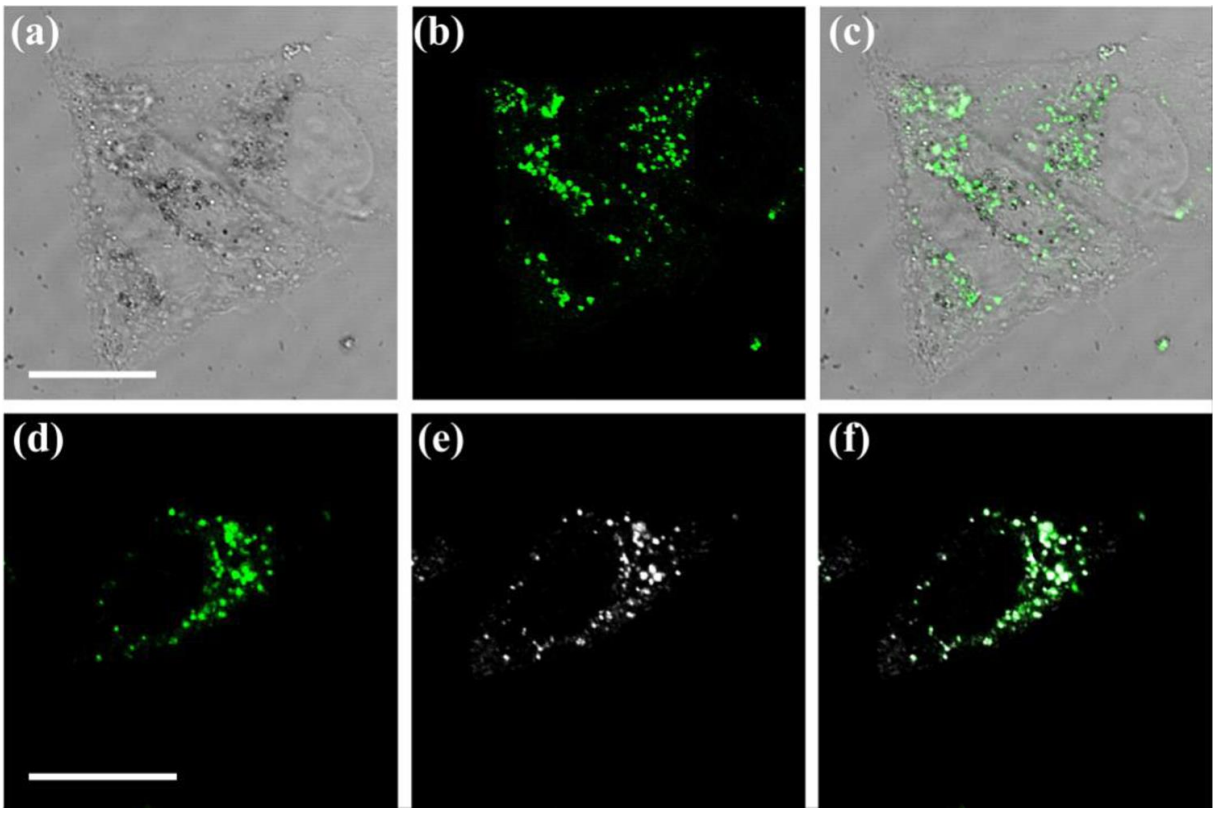

Figure 4. Optical imaging of A549 cells loaded with FND-Au after 24 h of incubation. (a) Bright field. (b) Fluorescence channel (green, λex = 561 nm and emission wavelength = 575−718 nm). (c) Overlap of (a) and (b). (d−f) Fluorescent and scattering imaging of FND-Au in A549 cells. (d) Fluorescence channel (green, λex = 561 nm and emission wavelength = 575−718 nm). (e) Scattering channel (gray, λex = 458 nm, scattering wavelength = 450−470 nm). (f) Overlap of (d) and (e). Scale bar: 20 μm.

Because free FNDs form aggregates after degradation of the biopolymer coating, the well-distributed hybrid particles found in TEM indicated that the biopolymer layer remained stable nd were still able to protect the inner FND-Au particles (Fig. S9a and d). After 24 h of incubation, single FND-Au and larger FND-Au coaggregates were found (Fig. S9b and e), suggesting that some protein polymer (HSA-PEO) coating could have started to degrade. However, the also thus-formed FND-Au coaggregates could be applied for cellular bioimaging

The presence of one or two AuNPs attached to the surface of the FNDs also enabled imaging via photothermal optical lock-in optical coherence microscopy (poli-OCM).[26] The poli-OCM provides 3D specific contrast images with excellent sensitivity by employing the photothermal contrast mechanism,[27] which benefits from the strong plasmonic resonance of AuNPs. HeLa cells incubated with FND-Au for 12h were imaged on the poli-OCM using both of its modalities. In the dark-field OCM mode, the entire 3D morphology of the cells was imaged (Fig. S6a), whereas the poli-OCM modality allowed specific intracellular imaging utilizing the AuNPs as localized heating zones thus providing high photothermal contrast.[26] A 532 nm laser was used to excite the plasmonic resonance of the Au inducing localized heating, essential for poli-OCM imaging (bandpass 735−865 nm). The same 532 nm laser also excited the FNDs and the resulting emission was acquired through the fluorescence arm of the poli-OCM. (Fig. S6b, HQ680/35m emission filter). We have identified the FND fluorescence and the photothermal signal from the AuNPs (Fig. S6b and c) clearly demonstrating that the FND-Au facilitated dual mode imaging with the fluorescence and photothermal channels.

According to these results, the FND-Au have been detected by emission, scattering and photothermal channels, thus forming a novel class of hybrid nanomaterials combining multimodal optical imaging with the greatest flexibility for selecting the desired detection methods as well as high sensitivity and efficient cellular uptake. However, limited by the resolution of optical microscopy (hundreds of nanometers), the even more detailed sub

organelle distribution or behavior of FND-Au could not be observed. Therefore, it would be highly desirable to extend the application of FND-Au to transmission electron microscopy (TEM) imaging, which could provide the highest resolution, down to the nanometer scale, for single FND-Au nanoparticle tracking in subcellular organelles.

Subcellular Organelle Electron Microscopy Imaging of FND-Au. TEM imaging provides higher spatial resolution compared to optical imaging techniques, but the contrast of the TEM images strongly depends on the thickness and composition of the sample material. Compared to heavy metal materials such as AuNPs, FNDs exhibited low contrast in TEM imaging due to the carbon crystal composition. Moreover, cellular sections need to be stained with uranyl acetate to enhance contrast, particularly in complicated subcellular environments, which makes it even more challenging to differentiate FNDs from the complex cellular components. In the past, only FND aggregates were differentiated from the cellular background, whereas in the case of single-FND detection, defocusing of the images or additional electron diffraction[13] had to be applied, which limited the application of FNDs for electron microscopy cellular imaging applications.

FND-Au hybrid nanoparticles provided high resolution and contrast in TEM, and single hybrid particles were easily localized inside cells (Fig. 5a), thus allowing the tracking of their cellular uptake, intracellular release, and trafficking with single-particle resolution. They localized in spherical endosomes (Fig. 5b) and in the cytosol (Fig. 5c). Interestingly, FND-Au localized in the cytosol were surrounded by many luminal vesicles similar to those found in endosomes (Fig. 5 b and c, marked with green circles) but lacking the associated endosome membrane, which indicated that these vesicles were the remains of disrupted endosomes. To further clarify this observation, FND-Au were also observed near the partially penetrated endosomal membrane and the disrupted membrane appeared perpendicular to the sharp edges of the FNDs (Fig. 5d and e, marked with red arrows). Some other images clearly revealed FND-Au hybrid

particles at the endosome pentration stage, with disrupted endosome membrane fragments nearby (Fig. S7a and b, marked with a blue circle) or altered organelle membrane morphology from globular to structurally deformed (Fig. S7c and d, marked with a red arrow), indicating endosomal membrane penetration of the FND-Au due to the sharp edges of FNDs. We have imaged the endosome release process of FNDs for the first time, clearly proving previous hypotheses that the sharp edges of FNDs were responsible for membrane release.[12] This important sub-organelle process was now imaged in such detail due to the presence of the AuNPs that allowed tracking of the FNDs by TEM with nanometer resolution in the complex cellular surroundings.

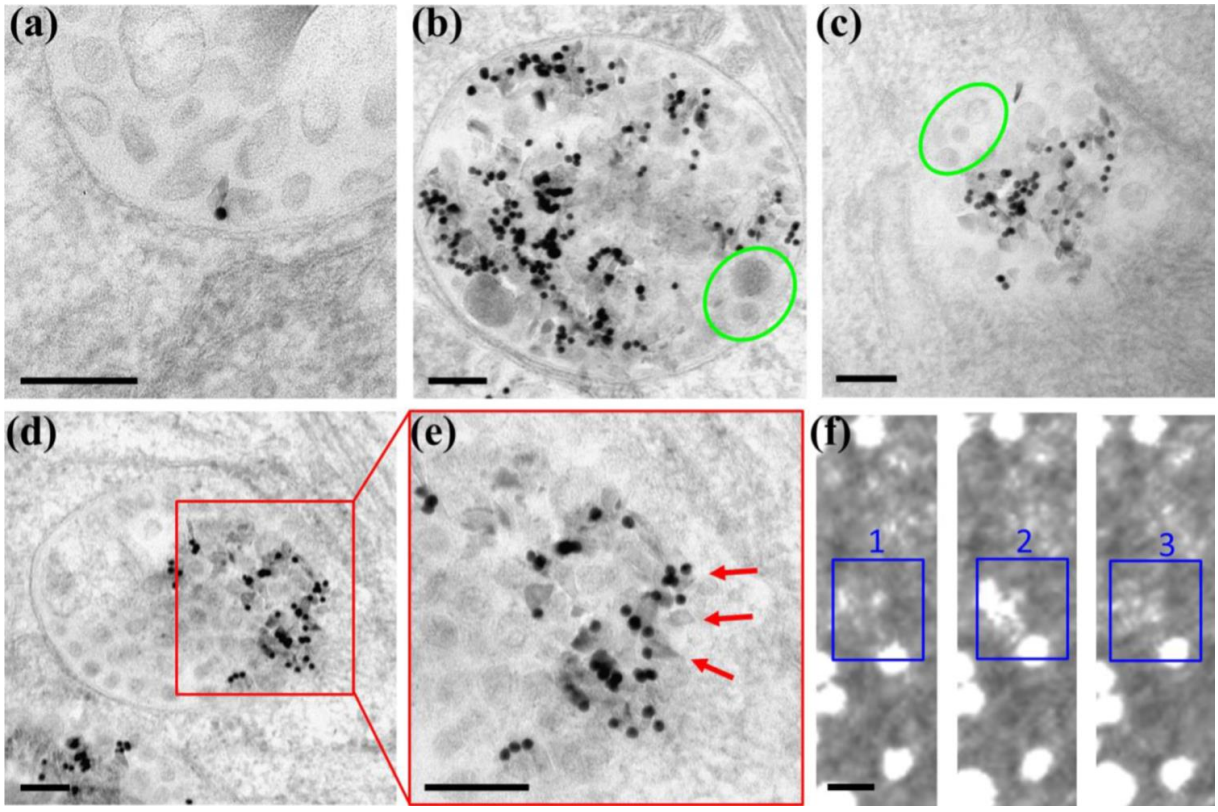

Figure 5. FND−Au cell distribution and cell slice observed by TEM based on the high-pressure freezing procedure.[30] (a) Single FND-Au inside the cellular endosome. (b, c) FND-Au distributed in endosomes and cytosol. (d) Disrupted endosome membrane by the sharp FND edges. (e) Amplification of (d). (f) STEM image tilt series with a 1.5° increment. Scale bar: (a−e) 100 nm and (f) 20 nm.

The cellular distribution of FND-Au was analyzed at different incubation times. After 12 h of incubation, FND-Au were mainly distributed inside endosomes (Fig. S8a, marked with blue squares), but their release into the cytosol occurred after an additional 12 h of incubation in fresh cell culture medium (Fig. S8b, marked with a red square). The observed endosomal disruption and cytosolic distribution could be explained by the extremely long cell retention of FNDs,[11] and these features are particularly relevant for cell tracking experiments over extended time periods.[28] The enhanced subcellular translocation through the endosome membrane penetration pathway, and the prolonged cell retention times were essential for the application of FND-Au, such as long-term bioimaging or intracellular drug release. Obviously, the distinctive features of the FNDs seemed to be responsible for the unique characteristics of the FND-Au hybrids in controlling endosomal release, subcellular migration, and retention.

The 3D morphology of the FND-Au endosome distribution was investigated by scanning and transmission electron microscopy tomography. The respective bright field images of reconstruction of the tilt series between -70° to 72° with 1.5° increments were depicted in the movie in the Supporting Information (20160311cDFreconstruction, horizontal field width 655 nm). A dark signal was obtained from the AuNPs that heavily scattered due to the high density of the AuNPs in the FND-Au. Consequently, the FNDs could not be detected in a single image because the density of the FNDs was lower than the density of the heavy metal stained biological structures. However, Bragg scattering enabled direct determination of the FNDs based on their extraordinary flickering behavior. As shown in Fig. 5f in the dark-field images of three consequent tilt series, the FND exhibited continuously appearing and disappearing motions during specimen rotation (marked by the blue squares). This so-called "flickering" effect was clearly observed in the movie in the Supporting Information (20160311cDFtilt_series, horizontal field width 655 nm). Bragg scattering critically depends on the angle of the crystal lattice and the incoming beam,[29] with small changes in this angle causing major changes in Bragg contrast. The Bragg scattered electrons were scattered to low angles and only hit the

dark-field detector when a long camera length was chosen. This results in "flickering" of the signal originating from the FNDs, when the images of the tilt series are viewed as a movie. Although the FND contrast was not very high in the movie, the blinking was well-distinguished from the static cellular back-ground. Because the STEM dark-field images were performed by electron transmission and scattering, the distinct flickering behavior was only related to the crystalline composition and structure of the FND in the hybrid particles. Consequently, following this method, nanodiamonds could even be observed with high spatial resolution inside cells in the absence of any NV emission to provide subcellular organelle information.

Conclusion:

We have presented the convenient and efficient preparation of FND-Au hybrid nanoparticles, and we have demonstrated their application as powerful markers for detailed cellular investigations with high precision. FND-Au offer many distinct features: (1) the FND-Au nanoparticles exhibited photostable emission originating from the FND and an optically active localized surface plasmon resonance from the AuNP entity, facilitating optical imaging in both the emission and the scattering modes without quenching of the FND emission by the AuNPs. (2) The AuNPs' surface plasmon resonance effect allowed the reduction of laser power, and consequently, less irradiation time was required for FND excitation, thus making the FND-Au particles well-suited for multimodal optical imaging with improved biocompatibility. (3) AuNPs labeling greatly improved the FND-Au contrast in TEM images, providing an additional electronic microscopy method to study the FND cellular migration and fate with single particle spatial resolution. (4) STEM dark-field tomography revealed flickering of the nanodiamonds inside cells for the first time, thus presenting an entirely new, 3D, and high-resolution approach to study nanodiamonds in such hybrid nanoparticles inside subcellular organelles.

We have shown that the optical excitation of NV centers was significantly improved by stabilizing gold nanoparticles in the closest distance from the FND surface. Therefore, this

hybrid technique offers great opportunities for nanoscale magnetic field sensing based on NV defects. Optical polarization of NV centers was achieved with lower excitation laser power, which allows the performance of cellular experiments with lower energy light, which is important for sensing applications inside cells.[31] Furthermore, plasmonic enhancement of luminescence via the Purcell effect[32] could be employed to improve the signal-to-noise measurements in diamond magnetometry.[33]

The great potential of FND-Au nanoparticles as markers and (quantum) sensors inside living cells is based on their efficient cellular uptake by endocytosis due to the positively charged polymer surface coating, their endosomal escape by the sharp FND crystal structures that partially destroyed the endosomal membranes, and their favorable cytotoxicity profile. Partial destruction of endosomal membranes could be attractive, for nanoparticle sensors introduced into living cells as globular nanoparticles without cellular translocation groups usually remain trapped inside endosomes. We have shown that this endosomal release process did not induce cytotoxicity, and the endosomal uptake and release pathways of living cells were

not negatively affected after incubation with FND-Au. As the FND-Au hybrids remained intact, even after 12 h of incubation inside living cells, they represent attractive candidates for cellular imaging studies over extended time periods.

We believe that the multimodal imaging capabilities of FND-Au will generate comprehensive images with enhanced sensitivity and flexible selection of the imaging mode to enable fast and reliable tracking of FND-Au and their interaction partners inside complex cellular environments with highest contrast and resolution. Moreover, the AuNPs used for the hybrid particle preparation could, in principle, be replaced by other nanoparticles of similar sizes. Thus, the preparation method described herein represents a versatile platform for generating various FND hybrid particle combinations, which allows further fine-tuning the optical properties and spin states of the FNDs. Additionally, drugs, proteins, or DNA-targeting groups could be introduced

to the outer protein coating, providing new avenues for tracking of the delivery of drug molecules or studying protein−protein or protein−DNA

interactions inside living cells.

ASSOCIATED CONTENT

Supporting Information. Detailed experimental information, additional optical-electronic imaging figures, STEM movies are in the supporting information. This material is available free of charge via the Internet at http://pubs.acs.org.

AUTHOR INFORMATION

Corresponding Author

*yuzhou.wu@uni-ulm.de, *tanja.weil@uni-ulm.de

ACKNOWLEDGMENT

This work has been supported by the ERC Synergy Grant 319130-BioQ grant and SFB 1149 grant (project A04 Barth/Weil). B.W. gratefully acknowledges support by the Braunschweig International Graduate School of Metrology B-IGSM and the DFG Research Training Group GrK1952/1 "Metrology for Complex Nanosystems". P.T acknowledges support by the Deutsche Forschungsgemeinschaft (TI 329/9-1). We thank Ms. Rose Rosenberg for analytical ultracentrifugation analysis of FND-Au. We thank Ms. Renate Kunz for cryo-cell section preparation and staining.

REFERENCES

1. Hsiao, W. W.-W.; Hui, Y. Y.; Tsai, P.-C.; Chang, H.-C. *Accounts of Chemical Research* **2016,** 49, (3), 400-407.
2. Fu, C.-C.; Lee, H.-Y.; Chen, K.; Lim, T.-S.; Wu, H.-Y.; Lin, P.-K.; Wei, P.-K.; Tsao, P.-H.; Chang, H.-C.; Fann, W. *Proc. Natl. Acad. Sci. U. S. A.* **2007**, 104 (3), 727-732.
3. Balasubramanian, G.; Neumann, P.; Twitchen, D.; Markham, M.; Kolesov, R.; Mizuochi, N.; Isoya, J.; Achard, J.; Beck, J.; Tissler, J.; Jacques, V.; Hemmer, P. R.; Jelezko, F.; Wrachtrup, *J. Nat. Mater*. **2009**, 8 (5), 383-387.
4. Neumann, P.; Jakobi, I.; Dolde, F.; Burk, C.; Reuter, R.; Waldherr, G.; Honert, J.; Wolf, T.; Brunner, A.; Shim, J. H.; Suter, D.; Sumiya, H.; Isoya, J.; Wrachtrup, J. *Nano Letters* **2013**, 13 (6), 2738−2742.
5. Wu, Y.; Jelezko, F.; Plenio, M. B.; Weil, T. *Angewandte Chemie International Edition* **2016**, 55 (23), 6586-6598
6. Ermakova, A.; Pramanik, G.; Cai, J. M.; Algara-Siller, G.; Kaiser, U.; Weil, T.; Tzeng, Y. K.; Chang, H. C.; McGuinness, L. P.; Plenio, M. B.; Naydenov, B.; Jelezko, F. *Nano Letters* **2013,** 13, (7), 3305-3309.
7. Lovchinsky, I.; Sushkov, A. O.; Urbach, E.; de Leon, N. P.; Choi, S.; De Greve, K.; Evans, R.; Gertner, R.; Bersin, E.; Müller, C.; McGuinness, L.; Jelezko, F.; Walsworth, R. L.; Park, H.; Lukin, M. D. *Science* **2016** 51 (6275), 836−841.
8. Arroyo-Camejo, S.; Adam, M.-P.; Besbes, M.; Hugonin, J.-P.; Jacques, V.; Greffet, J.-J.; Roch, J.-F.; Hell, S. W.; Treussart, F. *ACS Nano* **2013,** 7, (12), 10912-10919.
9. Tzeng, Y.-K.; Faklaris, O.; Chang, B.-M.; Kuo, Y.; Hsu, J.-H.; Chang, H.-C *Angewandte Chemie International Edition* 2011, 50 (10), 2262−2265.
10. Zhu, Y.; Li, J.; Li, W.; Zhang, Y.; Yang, X.; Chen, N.; Sun, Y.; Zhao, Y.; Fan, C.; Huang, Q. *Theranostics* **2012,** 2, (3), 302-312.
11. Vaijayanthimala, V.; Cheng, P.-Y.; Yeh, S.-H.; Liu, K.-K.; Hsiao, C.-H.; Chao, J.-I.; Chang, H.-C. *Biomaterials* **2012,** 33, (31), 7794-7802.
12. Chu, Z.; Zhang, S.; Zhang, B.; Zhang, C.; Fang, C.-Y.; Rehor, I.; Cigler, P.; Chang, H.-C.; Lin, G.; Liu, R.; Li, Q. *Scientific Reports* **2014,** 4, 4495.
13. Zurbuchen, M. A.; Lake, M. P.; Kohan, S. A.; Leung, B.; Bouchard, L.-S. *Scientific Reports* **2013,** 3, 2668.
14. Iwasashi, M.; Sakane, M.; Saito, H.; Taguchi, T.; Tateishi, T.; Ochiai, N. *J. Biomed. Mater. Res*., *Part A* **2009**, 90A (2), 543-548.
15 Koynov, K.; Butt, H.-J. *Current Opinion in Colloid & Interface Science* **2012,** 17, (6), 377-387.
16. Acuna, G. P.; Möller, F. M.; Holzmeister, P.; Beater, S.; Lalkens, B.; Tinnefeld, P. *Science* **2012,** 338, (6106), 506-510.
17. Giannini, V.; Fernández-Domínguez, A. I.; Heck, S. C.; Maier, S. A. *Chemical Reviews* **2011,** 111, (6), 3888-3912.
18. Acuna, G. P.; Bucher, M.; Stein, I. H.; Steinhauer, C.; Kuzyk, A.; Holzmeister, P.; Schreiber, R.; Moroz, A.; Stefani, F. D.; Liedl, T.; Simmel, F. C.; Tinnefeld, P. *ACS Nano* **2012,** 6, (4), 3189-3195.
19. Berthel, M.; Mollet, O.; Dantelle, G.; Gacoin, T.; Huant, S.; Drezet, A. *Physical Review B* **2015,** 91, (3), 035308.
20. Ul, N. *Biochimica et Biophysica Acta (BBA) - Protein Structure* **1971,** 229, (3), 567-581.
21. Wu, Y.; Ermakova, A.; Liu, W.; Pramanik, G.; Vu, T. M.; Kurz, A.; McGuinness, L.; Naydenov, B.; Hafner, S.; Reuter, R.; Wrachtrup, J.; Isoya, J.; Förtsch, C.; Barth, H.; Simmet, T.; Jelezko, F.; Weil, T. *Advanced Functional Materials* **2015,** 25, (42), 6576-6585.

22. Murphy, C. J.; Gole, A. M.; Stone, J. W.; Sisco, P. N.; Alkilany, A. M.; Goldsmith, E. C.; Baxter, S. C. *Accounts of Chemical Research* **2008,** 41, (12), 1721-1730.
23. Barth, H.; Blöcker, D.; Behlke, J.; Bergsma-Schutter, W.; Brisson, A.; Benz, R.; Aktories, K. *J. Biol. Chem.* **2000**, 275 (25), 18704−18711.
24. Niidome, T.; Yamagata, M.; Okamoto, Y.; Akiyama, Y.; Takahashi, H.; Kawano, T.; Katayama, Y.; Niidome, Y. *Journal of Controlled Release* **2006,** 114, (3), 343-347.
25. Nowacek, A.; Kadiu, I.; McMillan, J.; Gendelman, H. E. Methods
Mol. Biol. 2013, 991, 47-55.
26. Pache, C.; Bocchio, N. L.; Bouwens, A.; Villiger, M.; Berclaz, C.; Goulley, J.; Gibson, M. I.; Santschi, C.; Lasser, T. *Optics express* **2012,** 20, (19), 21385-21399.
27. Boyer, D.; Tamarat, P.; Maali, A.; Lounis, B.; Orrit, M. *Science* **2002,** 297, (5584), 1160-1163.
28. Taylor, A.; Wilson, K. M.; Murray, P.; Fernig, D. G.; Lévy, R. *Chemical Society Reviews* **2012,** 41, (7), 2707-2717.
29. Reimer, L., *Transmission electron microscopy: physics of image formation and microanalysis*. Springer: 2013; Vol. 36.
30. Höhn, K.; Sailer, M.; Wang, L.; Lorenz, M.; Schneider, M. E.; Walther, P. *Histochemistry and cell biology* **2011,** 135, (1), 1-9.
31. McGuinness, L. P.; Yan, Y.; Stacey, A.; Simpson, D. A.; Hall, L. T.; Maclaurin, D.; Prawer, S.; Mulvaney, P.; Wrachtrup, J.; Caruso, F.; Scholten, R. E.; Hollenberg, L. C. L. *Nat. Nanotechnol*. **2011**, 6 (6), 358−363.
32. Purcell, E. M.; Torrey, H. C.; Pound, R. V. *Phys. Rev*. **1946**, 69 (1−2), 37−38.
33. Wolf, S. A.; Rosenberg, I.; Rapaport, R.; Bar-Gill, N. *Phys. Rev. B: Condens. Matter Mater. Phys.* **2015**, 92 (23), 235410.